

## Effect of cellulose compositions and fabrication methods on mechanical properties of polyurethane-cellulose composites

Tzu-Yi Yu<sup>a,1</sup>, Yu-Kai Tseng<sup>a,1</sup>, Ting-Han Lin<sup>b</sup>, Tzu-Chia Wang<sup>a</sup>, Yun-Hsiu Tseng<sup>a</sup>, Yin-Hsuan Chang<sup>b</sup>, Ming-Chung Wu<sup>b,c,d,\*</sup>, Wei-Fang Su<sup>a,e,f,\*\*</sup>

<sup>a</sup> Department of Materials Science and Engineering, National Taiwan University, Taipei 10617, Taiwan

<sup>b</sup> Department of Chemical and Materials Engineering, Chang Gung University, Taoyuan 33302, Taiwan

<sup>c</sup> Green Technology Research Center, Chang Gung University, Taoyuan 33302, Taiwan

<sup>d</sup> Division of Neonatology, Department of Pediatrics, Chang Gung Memorial Hospital at Linkou, Taoyuan 33305, Taiwan

<sup>e</sup> Molecular Imaging Center, National Taiwan University, Taipei 10617, Taiwan

<sup>f</sup> Department of Materials Engineering, Ming Chi University of Technology, New Taipei City 24301, Taiwan

### ARTICLE INFO

#### Keywords:

Cellulose nanofiber  
Ethyl cellulose  
Polyurethane  
Nanocomposite  
Microstructure-property relationship  
Composition  
Morphology

### ABSTRACT

A variety of cellulose-based polymer composite materials has been developed and show different impacts on the morphologies and properties of composites. Herein, we report the morphologies and properties of composites by blending polyurethane (PU) with either ethyl cellulose (EC) or cellulose nanofiber (CNF) through either drop-casting or electrospinning process. EC is homogeneously mixed with PU without microphase separation and enhanced Young's modulus of composites from 0.04 to 6.94 MPa. The CNF is heterogeneously distributed in PU/CNF composites without interference on the PU microstructure and slightly increased modulus to 0.24 MPa. While the shearing force of the electrospinning process slightly affects the PU/EC composites, it drastically enhances PU crystallinity and Young's modulus to 54.95 MPa in PU/CNF composites. A model is established to summarize the effect of cellulose additives, compositions, and processes on PU/cellulose composites, providing a comprehensive understanding for designing future cellulose composites.

### 1. Introduction

A key challenge for applying electrospun polyurethane in cardiac tissue engineering is the soft and elastic characteristics that often result in non-uniform fiber with beads, intertwining and sticky together (Su et al., 2016). Polymer blending is seen as a cost-effective method to modify the properties of soft materials. Polymer blend is a mixture of two or more polymers without covalent chemical bonding, and it can be classified into 2 categories: miscible polymer blend and immiscible polymer blend. A miscible polymer is a single-phase structure where two or more polymers are mixed homogeneously with each other, and it exhibits one glass transition temperature. Dong et al. prepared a poly (lactic acid)/ethyl cellulose/hydroxyapatite (PLA/EC/HA) scaffold, where the precursor solution is uniform and stable suspension. The scaffolds show increased mechanical properties due to the compact and intact porous architecture (Mao et al., 2018). In contrast, immiscible

blend is a mixture made from two polymers that shows separate phases, and their respective glass transition temperatures are observed. Sakakibara et al. proposed an effective approach to blended hydrophilic cellulose nanofibers into hydrophobic high-density polyethylene (HDPE) by adding a diblock copolymer dispersant. They found the degree of dispersion strongly affected the extent of reinforcement in mechanical properties (Sakakibara et al., 2016).

As the main component for constructing the cell wall in all plants, cellulose is abundant in nature (Seddiqi et al., 2021). Besides its easy access, its extraordinary mechanical strength and stability make it a vital material in the developmental history of humankind. Cellulose has been burned as an energy resource and made into long-lasting materials, such as paper for word recording and an indispensable component for constructing daily apparatus and housing. By functionalizing into polymeric derivatives or nanomaterials with physical and chemical modifications, cellulose extends its importance in academic research and industrial

\* Correspondence to: M.-C. Wu, Department of Chemical and Materials Engineering, Chang Gung University, Taoyuan 33302, Taiwan.

\*\* Correspondence to: W.-F. Su, Department of Materials Science and Engineering, National Taiwan University, Taipei 10617, Taiwan.

E-mail addresses: [mingchungwu@cgu.edu.tw](mailto:mingchungwu@cgu.edu.tw) (M.-C. Wu), [suwf@ntu.edu.tw](mailto:suwf@ntu.edu.tw) (W.-F. Su).

<sup>1</sup> Equal contribution as the first author.

<https://doi.org/10.1016/j.carbpol.2022.119549>

Received 8 December 2021; Received in revised form 5 April 2022; Accepted 26 April 2022

Available online 30 April 2022

0144-8617/© 2022 Elsevier Ltd. All rights reserved.

application with great potential beyond its current usage.

Cellulose is robust and impact-enduring because of its molecular structure. Cellulose, composed of glucose units, exhibits many hydroxyl and ether groups providing numerous acceptors and donors of hydrogen bonds. The intermolecular interaction and symmetric conformation have resulted in a close-packed structure of cellulose with high crystallinity (Nishiyama et al., 2002; Nishiyama et al., 2003). On the contrary, the processibility of cellulose is limited because the strong hydrogen bond makes it insoluble in water or organic solvent. The hydroxyl group in cellulose has been modified into various functional groups, such as acetate, ether with aliphatic chain, and charged ionic groups to promote its solubility (Fox et al., 2011; Seddiqi et al., 2021). These polymeric cellulose derivatives are popular candidates for composite materials due to their high solubility, chemical stability, and mechanical robustness. Ethyl cellulose (EC) has been reported to contribute to the robustness and stability of a blended matrix as the functional separator in lithium-ion batteries (Zuo et al., 2018). A porous composite material containing EC has been shown to promote bone regeneration (Mao et al., 2018). Polymeric additives of cellulose have been broadly used to support functional materials (Lu & Yuan, 2018; Mao et al., 2018) or blend with a softer counterpart, such as polyurethane (PU), to balance the stiffness and elongation of their composite (Chen et al., 2015; Su et al., 2016). These polymeric cellulose derivatives have also been used as essential materials in various industries, including food, pharmaceutical, energy, coating, etc. (Seddiqi et al., 2021).

Recently, cellulose nanomaterial has raised great attention among academic and industrial researchers. Through various chemical and mechanical treatments, cellulose can be fabricated into either cellulose nanocrystal (CNC), a nanorod comprised of fully crystalline cellulose, or cellulose nanofiber (CNF), a nanofiber containing both amorphous and crystalline cellulose (Chu et al., 2020; Seddiqi et al., 2021). The surfaces of these cellulose nanomaterials can be modified with charged functional groups to stabilize their ability to suspend in aqueous solutions. Despite the differences in preparation methods and structures, these cellulose nanomaterials exhibit a high aspect ratio, toughness, and tunable surface chemistry. Currently, they are the prevailing candidates in nanocomposite research. Besides acting as a robust nano-filler, cellulose nanomaterial extends its structural complexity and potential in numerous applications with the formation of higher-order hierarchical structures, such as a CNF network. A high concentration of CNF aqueous suspension has been transformed into a hydrogel, a water-filled network with moderate stiffness against external forces. This CNF hydrogel, as an analog to extracellular matrix in organisms, has demonstrated its potential in tissue engineering and regenerative medicine (Basu et al., 2017; Chen et al., 2019; Xu et al., 2020; Ye et al., 2018). The cellulose nanofiber network formation has also shown its efficacy in promoting the mechanical strength of such nanocomposite materials (Cheng et al., 2016). Due to their superior physical properties, tunable surface chemistry, and relatively easy access compared to graphene and carbon nanotubes, cellulose nanomaterials are perspective nanomaterials in nanoscience and nanocomposite materials.

Although cellulose has been modified by various functional groups into different forms and has been widely used in designing materials, the effect of cellulose functional groups on composite materials is rarely investigated and discussed. Unfortunately, the diversities of the composite system and the differences in preparing methods of cellulose materials make it hard to compare the results between different reports. Herein, we explore the effect of various types of cellulose additives, their weight ratios, and the fabrication methods on the composition-structure-properties relationship using polyurethane (PU) and cellulose composites. The composites are prepared by blending either EC, a polymeric cellulose additive (Chen et al., 2015; Su et al., 2016), or CNF, a cellulose nanofiber additive, in the PU matrix. These composites are fabricated into drop-casted films to be investigated. To look into the complicated interaction between PU and cellulose additives under

external shear forces, these composites are studied as nanofiber scaffolds prepared by the electrospinning process. We hypothesize that only EC would interfere with PU microphases. We also expect that electrospinning would enhance the crystallinity of PU and the mechanical strength in both PU/EC and PU/CNF composite scaffolds. This research clarifies the effects of cellulose type, composition, and fabrication method on the microstructure and the mechanical properties of PU/cellulose composites under comparable conditions. The results provide guidelines for the future design and fabrication of composite materials containing cellulose additives.

## 2. Materials and methods

### 2.1. General statement

Poly-caprolactone diol (PCL diol, Mw ~2000, 99+%), isophorone diisocyanate (IPDI, 97%), 1,4-diaminobutane (Putrescine, 99%), tetrahydrofuran (THF, 99.7%), and dimethylacetamide (DMAc, 99.5%) were purchased from Acros Chemical Company. Dibutyltin dilaurate (DBTDL, ~95%), ethyl cellulose (EC, 48.0–49.5% (w/w) ethoxy basis, 99+%), and *N,N*-dimethylformamide (DMF, 99.5%) were purchased from Sigma-Aldrich Chemical Company. All chemicals were used as received without further purification unless specified below.

PCL diol was dried under vacuum at 80 °C for more than 12 h. IPDI and DBTDL were dried under vacuum with stirring at room temperature for 12 h. Putrescine and DMF were dried with a molecular sieve and purged with N<sub>2</sub> (g).

### 2.2. Nomenclature

The various composites are labeled as either PU/EC or PU/CNF. The amount of EC or CNF in weight percentage is added to the name of each composite. For example, a PU/EC composite containing 10.0 wt% of EC is labeled PU/EC-10, and a PU/CNF composite containing 1.0 wt% of CNF is labeled PU/CNF-1.0.

### 2.3. Synthesis of urea terminated poly-urethane (PU)

For the synthesis of urea terminated poly-urethane, 6.0 g of PCL diol was dissolved in 40.0 ml of dried DMF in a 100.0 ml three-neck round bottom flask at 70 °C. 1.33 g of IPDI and 0.085 g of DBTDL were dissolved in 5.0 ml of dried DMF in a 25.0 ml double-neck round bottom flask. IPDI and DBTDL solution was quickly transferred into the PCL diol solution. The reaction was carried out at 70 °C for 5 h, and then the PCL diol solution was cooled down to room temperature. 0.278 g of putrescine was dissolved in 5.0 ml dried DMF and added drop-by-drop into the PCL diol solution over 30 min of chain-extension reaction. The reaction solution was poured into deionized water to stop the reaction and precipitate the product, PU. The product was dried in vacuum at 30 °C to remove any remaining solvent.

### 2.4. Synthesis of cellulose nanofiber (CNF) hydrogel

CNF was synthesized using the TEMPO-mediated oxidation method. Paper pulp (Chung Hwa Pulp Corporation) was chosen as raw material. The paper pulp contains nearly 98.9% cellulose, <0.5% hemicellulose and lignin, measured by a thermogravimetric analyzer (Q50, TA Instruments). First, the pulp was treated with dilute HCl at 100 °C for 2 h. Then, it is washed to reach a neutral pH. 0.025 g of 2,2,6,6-Tetramethylpiperidine-1-oxyl (TEMPO, Acros, 98%) and 0.250 g of sodium bromide (NaBr, Acros, 99.5%) were dissolved in 200.0 ml of deionized water, and 1.0 g of pulp was added. Then, 0.08 mol of sodium hypochlorite (NaClO, Choneye, 12%) was gradually mixed into the pulp suspension solution. The mixture was titrated to a pH close to 10 with 0.5 M NaOH and NaHCO<sub>3</sub> for 24 h. 0.04 g sodium thiosulfate pentahydrate (Na<sub>2</sub>S<sub>2</sub>O<sub>3</sub>·5H<sub>2</sub>O, Acros, 99.5%) and 1.0 ml ethanol were added to

terminate the oxidation. Sodium borohydride (NaBH<sub>4</sub>, Acros, 98+%) was added to eliminate the undesirable C<sub>6</sub> aldehydes and C<sub>2</sub>/C<sub>3</sub> ketones. Lastly, CNF hydrogel was washed several times and collected by centrifugation.

The surface charge of CNF is characterized by Zetasizer (Malvern, Zetasizer Nano ZS). The CNF hydrogel was diluted to 0.5 wt% in deionized water into an aqueous suspension. At pH 7.0, its Zeta potential is  $-51.9 \pm 6.4$  mV. The average diameter of as-prepared CNF was around  $18.1 \pm 2.2$  nm, and the corresponding aspect ratio was around 65 (Lin et al., 2021). For the study of percolation threshold, we followed the simplicity form of percolation model (Redondo et al., 2022), to evaluate the critical volume fraction of CNF in PU/CNF drop film. The critical volume fraction is around 0.70 vol%, equal to 0.70 wt%. This value is lower than the optimal PU/CNF-1 drop film which showed the critical modulus. It indicates that the increasing blend concentration of CNF improves the CNF network construction and then reinforcing the mechanical properties (Pei et al., 2011).

### 2.5. Preparation of PU/EC blending films

The dried PU and EC were dissolved in THF and stirred at 37 °C for 12 h. The solutions were drop-casted in Petri dishes and dried at room temperature in a hood to prepare PU/EC blending films. The PU/EC weight ratio ranged from 1.0 to 0.0, corresponding to the PU/EC samples listed in Table S1.

### 2.6. Preparation of PU/CNF nanocomposite films and electrospun scaffolds

Through the solvent exchange method, the CNF aqueous suspension was changed into CNF THF suspension. The CNF aqueous suspension was added to an equal amount of THF and mixed by a sonicator. Then, the mixed suspension was centrifuged. After removing the supernatant, CNF was re-suspended with THF. The process was repeated more than five times. To prepare electrospun scaffolds, CNF was finally suspended in DMAc instead.

To fabricate drop-casted film, the dried PU was mixed with CNF suspension in THF and stirred at 37 °C for at least 12 h. The mixed liquid was dropped in Petri dishes and dried at room temperature. The weight percentage of CNF ranged from 0.5 to 4.0 in total solid content, corresponding to the PU/CNF samples listed in Table S1.

The electrospun liquid was prepared by mixing dried PU and CNF in DMAc/THF (4,6 v/v) co-solvent with 25.0 wt% solid content. The mixed liquid was filled into a 3.0 ml syringe (24-gauge, Terumo, USA). The PU/EC scaffolds were electrospun at an applied voltage of 28.0 kV, a flow rate of 0.3 ml/h, and a working distance of 15.0 cm. The PU/CNF scaffolds were electrospun at an applied voltage of 20.0 kV, a flow rate of 0.3 ml/h, and a working distance of 15.0 cm. The isotropic scaffolds were collected by plate collector at a spin rate of 350 rpm. The anisotropic scaffolds were collected by drum collector at a spin rate of 2800 rpm.

### 2.7. Scanning electron microscopic study of scaffolds

The morphologies of electrospun scaffolds were characterized by SEM (JEOL, JSM-6510). The samples were sputter-coated with platinum at 20 mA for 60 s. The morphologies were observed at 1000× and 4000× magnification at 10 kV working voltage.

### 2.8. Differentiated scanning calorimetry (DSC) of PU-containing films and scaffolds

The microstructure of PU-containing composite films and scaffolds were quantitatively investigated by DSC (TA Instrument, Q200) with 1.0–2.0 mg of each sample. The furnace was heated up to 300 °C to remove moisture for 30 min. After cooling down to room temperature, a

sample was loaded into the furnace. All samples were scanned from –70 to 280 °C at 10 °C/min.

### 2.9. Grazing incidence wide-angle X-ray scattering (GIWAXS) of PU-containing films and scaffolds

The angstrom-level microstructure of PU-containing films and scaffolds was characterized by GIWAXS at the 13A work station in Taiwan's National Synchrotron Radiation Research Center (NSRRC). The samples were placed on sliced silicon wafers. At an incident angle of 0.2°, the scatter signal from 1 to 2 Å<sup>-1</sup> is integrated as a function of azimuth angle, and the degree of anisotropy is calculated as follows:

$$\text{Degree of anisotropy} = \frac{I_{\text{peak}}}{I_{\text{total}}} \times 100\%$$

where  $I_{\text{peak}}$  is the accumulated intensity at  $\pm 10^\circ$  azimuth angle when the peak orientation is set at  $0^\circ$ .  $I_{\text{total}}$  is the total intensity from 1 to 2 Å<sup>-1</sup> containing the signals of EC crystal, PU crystal, and separated phases of PU.

### 2.10. Universal tensile testing of PU-containing films and scaffolds

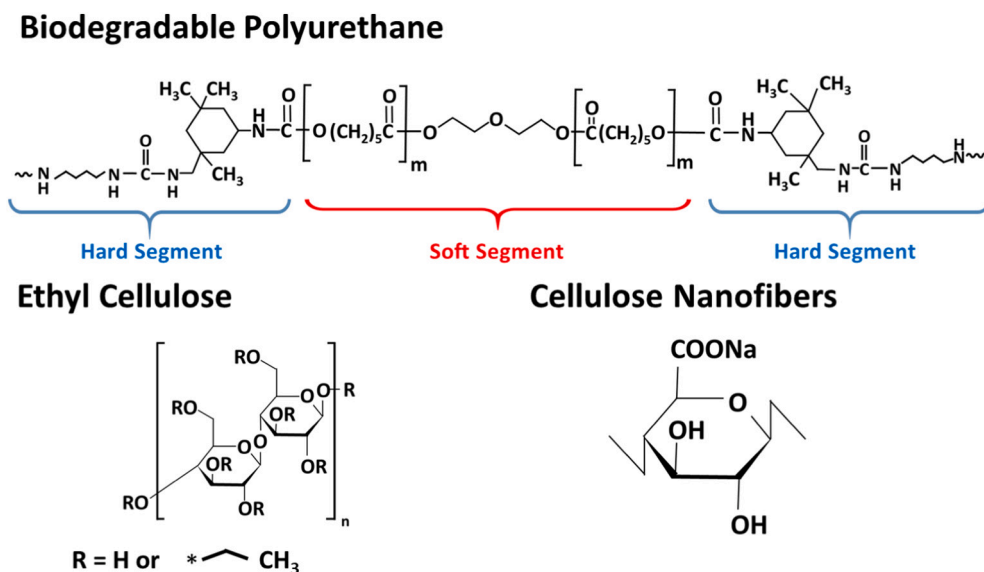
The PU-containing films and scaffolds were sliced into 1 cm by 5 cm rectangles for tensile testing (MTS Criterion 42.503 Test System). For each material, three samples were prepared for thickness measurement and tensile test. The thickness of samples was measured by a micrometer caliper. Two types of load: 5 N and 250 N were used to do the tensile testing depending on the mechanical strength of the material. The tests were carried out under ambient conditions with a 50 mm/min strain rate until breakdown.

## 3. Results and discussion

Ethyl cellulose used in this study was purchased from Sigma-Aldrich, which contained 48.0–49.5 wt% ethoxy group and 50.5–52.0 wt% hydroxy group. The urea terminated PU was synthesized through condensation polymerization. The isocyanate group of isophorone diisocyanate was reacted with polyol first, then reacted with amine chain extender, putrescine. Thus, there was no isocyanate left to react with the hydroxy group of EC (Su et al., 2016). On the other hand, CNF was prepared by the TEMPO-mediated oxidation method (Saito et al., 2007) at pH value of 10. The typical content of carboxyl group was near 1.50 mmol/g. At the pH of 10, there is no active hydrogen in CNF to react with PU. The carboxylates of CNF are likely to form hydrogen bonds but not covalent bonds with PU. The chemical structures of the PU, EC, and CNF are shown below (Scheme 1).

### 3.1. The effect of EC blending on the microstructure and mechanical properties of PU films

The PU/EC blend composite films are prepared by drop-casting the tetrahydrofuran solution. The details of film preparation are described in the Materials and methods section. Grazing incident wide-angle X-ray scattering (GIWAXS) was employed to characterize the microphase of PU/EC composite films. The 2D scatter pattern and integrated intensity are shown in Fig. 1(a) and (b). The halo signal of pure PU with maximum intensity at around 1.4 Å implies the PU phase separation of hard and soft segments, which happens naturally for most PUs. Pure EC shows two signals at around 0.6 and 1.4 Å, representing the crystalline phase of EC (Yuan et al., 2016). Fig. 1(a) shows that the signal intensity at 0.6 Å is proportional to the EC weight ratio, indicating that EC is well mixed in the PU matrix. The phase separation of PU, suggested by the signal at 1.4 Å, is suppressed by the presence of EC. Differential scanning calorimetry (DSC) results, shown in Fig. 1(c), also support this hypothesis. Contrasting to a strong endothermic signal of pure PU, PU/EC blend



Scheme 1. Chemical structure of PU, PE, and CNF.

films lose the phase transition signal at around 50 °C, indicating a homogenous mixture of PU/EC. Also, in <sup>13</sup>C solid-state NMR, the chemical signals of both EC and PU reach their maximum up-shift when the PU/EC weight ratio approaches (Fig. S1). Up-shifting in NMR means a higher shielding effect on the target atom, which is also a sign of the short distance to adjacent molecules. This phenomenon demonstrates the strong interaction between EC and PU for polymers rich in hydrogen bond donors and acceptors. In brief, EC could be homogeneously mixed with both the hard and the soft segment of PU on the molecular scale, thus hindering the microphase separation of PU in their blended films.

The mechanical properties of the PU/EC blended films are characterized by tensile testing. The Young's modulus, tensile strength, and elongation are plotted against the EC weight ratio in Fig. 2. The Young's modulus, tensile strength, and elongation of PU/EC nanocomposite films are listed in Table S1. The listed values in the table were obtained from the average data of the measurements from three samples of each material. As the EC weight ratio increases, the blended films perform better on the tensile strength and Young's modulus but decrease strain rate. The addition of EC enhances the mechanical strength of PU/EC composite films, which might be attributed to hydrogen bonding. The bulky glucose unit of EC might also curb the chain movement during deformation. The PU/EC films exhibit a wide range of Young's modulus, ranging from 0.04 to 6.94 MPa, and tensile strength, ranging from 7.0 to 19.8 MPa, shown in Fig. 2. In response, the addition of EC significantly reduces the elongation of PU/EC composite films, especially at a high EC weight ratio. The elongation of PU/EC films containing more than 50.0 wt% EC is two-order lower than the pristine PU film. The non-linear relation between Young's modulus and EC composition is similar to a reported plastics/elastomer blend (Liang & Ma, 2012). There is no evidence showing the correlation between the microstructural change and non-linear increase in Young's modulus after adding EC. In summary, EC is miscible with PU and proves to be an effective additive providing a wide range of Young's modulus, from 0.04 to 6.94 MPa, while drastically reducing the elongation of PU/EC blended films.

### 3.2. The effect of CNF nanocomposite on the microstructure and mechanical properties of PU films

PU/CNF nanocomposite films are fabricated using the same liquid casting procedure as PU/EC blended films. Using the same methods for EC/PU blended films, the microstructure of PU/CNF nanocomposite films was investigated by GIWAXS and DSC (Fig. 3), and the thermal

properties are summarized in Table S2. The nanocomposite effect of CNF on PU microstructure is drastically different from that of EC. Other than the high 4.0 wt% CNF, the addition of CNF in the PU matrix has no significant effect on the scattering pattern in GIWAXS and the endothermic peak in DSC. The phase separation of PU is unaffected by the additive of CNF unless a large amount of CNF is added. When the amount of CNF reached 4.0 wt%, its effect on microstructure became detectable in both GIWAXS and DSC. The formation of agglomerate or network of CNF could be the reason for this unique composite structure correlation. The microstructure details are further discussed after characterizing the mechanical properties of PU/CNF composite films.

Overall, the addition of less than 4.0 wt% of CNF endowed tremendous enforcement on the mechanical strength of its PU nanocomposite, which agrees with most of the literature report. Fig. 4(a)–(c) presents Young's modulus, tensile strength, and elongation of PU/CNF nanocomposite films versus CNF weight ratio, respectively. The Young's modulus, tensile strength, and elongation of PU/CNF nanocomposite films are listed in Table S1. The listed values in the table were obtained from the average data of the measurement from three samples of each material. The mechanical improvement mainly relies on the high aspect ratio and self-aligned structure of CNF. PU/CNF-2.0 has the highest Young's modulus of up to 0.24 MPa. PU/CNF-1.0 exhibits the best performance in tensile strength at 11.4 MPa, which is slightly higher than that of PU/CNF-2.0 film at 10.4 MPa. The enforcement effect in PU/CNF-4.0 is lower in every aspect compared to PU/CNF-2.0. Although the strain rate drops with increasing CNF, the PU/CNF nanocomposite maintains good elongation while enhancing its mechanical strength.

The changes of mechanical properties of PU/CNF (>1.0 wt% CNF) are consistent with the observations in DSC and WAXS, which might be due to the agglomerate or network formation of CNF in the PU matrix. The network formation of fibril cellulose is vital to the reinforcement effect on their nanocomposite films (Cheng et al., 2016; Iwatake et al., 2008; Xu et al., 2013). It was first proposed in polylactic acid (PLA) films reinforced by cellulose nanofibers in 2008. For higher than 10.0 wt% CNF in PLA films, the modulus of the film remained at a certain level when the PLA was placed above the glass transition temperature, suggesting as evidence of CNF network formation (Iwatake et al., 2008). This phenomenon was also reported in polyethylene oxide films (Xu et al., 2013). In the case of polyurethanes, Dong Cheng et al. in 2017 found that 1.0 wt% CNF aggregates into a network, which is consistent with the result from a numerical model based on solubility parameters of CNF in PU (Cheng et al., 2016). When the CNF weight ratio surpassed a

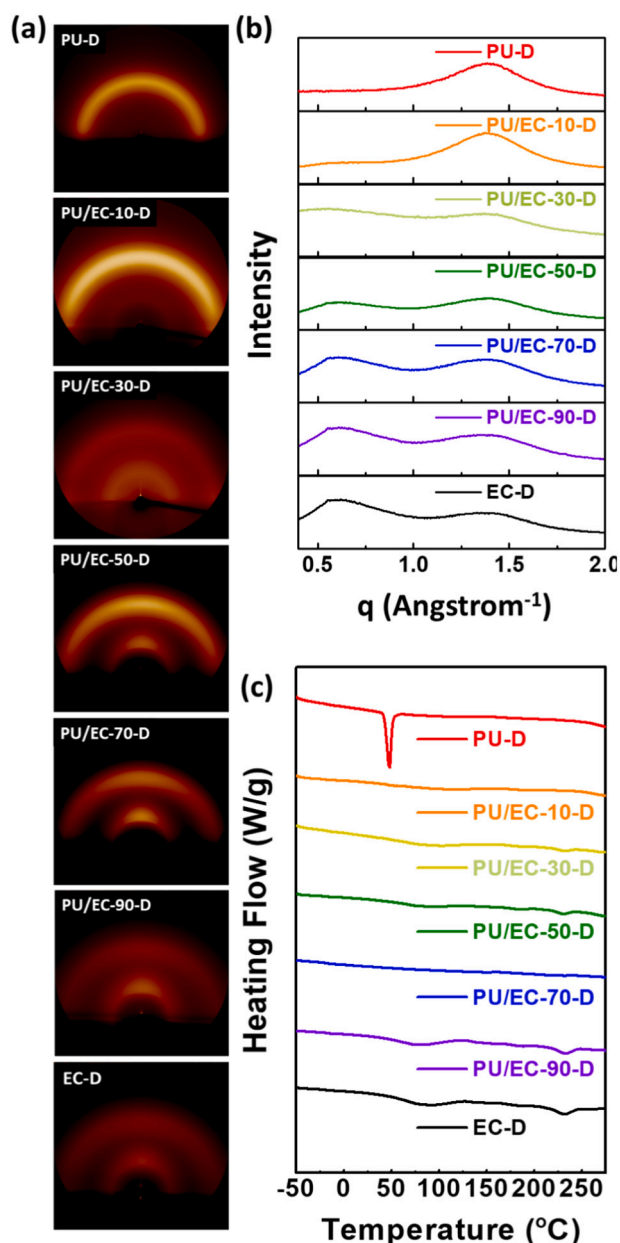


Fig. 1. Morphology studies of PU/EC blended films (a) 2D GIWAXS (b) integrated GIWAXS intensity versus  $q$  value. (c) DSC results at the first heating scan, showing phase separation being largely suppressed by blending EC in the PU matrix.

critical concentration at around 1.0 wt%, a CNF network was formed, and the enforcement on Young's modulus of the film abruptly arose. However, the critical concentration for CNF network formation can be controlled by many solubility-related parameters, such as the chemical structure of a matrix, fabrication methods, aspect ratio, and surface chemistry of CNF. Therefore, the threshold value at which CNF interconnection begins differs case-by-case. For our PU/CNF nanocomposite films, the aforementioned results are insufficient to postulate the specific CNF concentration at which a network is formed. This part of the discussion is further elaborated in the next section, with more results from PU nanocomposite scaffolds fabricated by the electrospinning method.

All these groups are in agreement with the changes in mechanical properties of CNF/polymer composite due to CNF agglomeration in a polymer matrix (Cheng et al., 2016; Iwatake et al., 2008; Xu et al.,

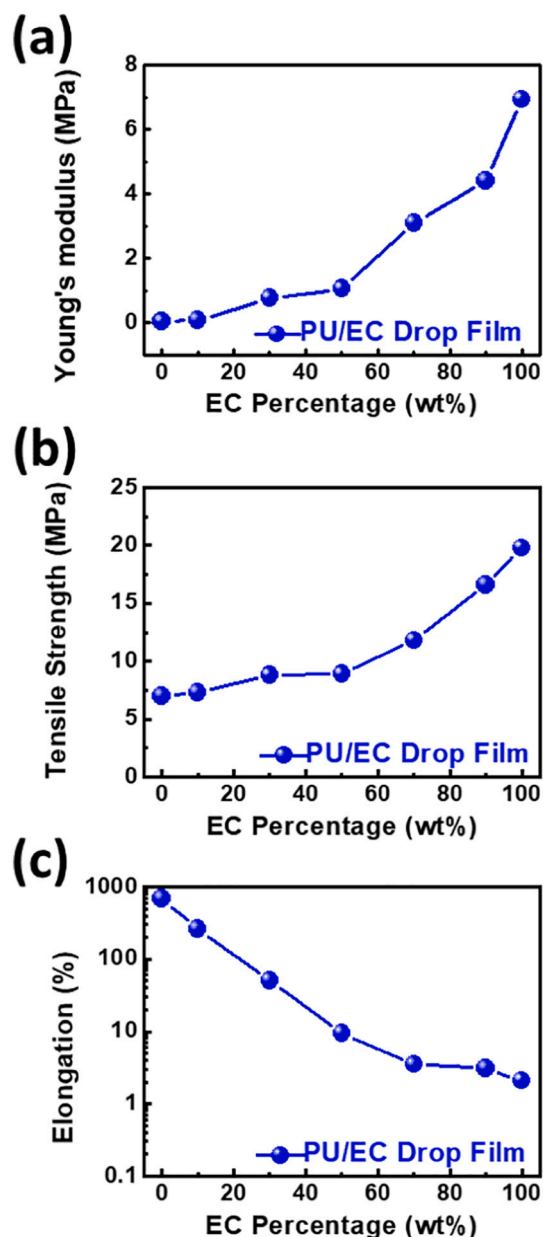


Fig. 2. Plots of mechanical properties versus EC concentration of PU/EC composite films (a) Young's modulus (b) tensile strength, and (c) elongation.

2013). For instance, Xuezhu Xu et al. suggested that if CNF concentration is higher than 10.0 wt%, CNF forms agglomerates in polyethylene glycol (PEO) film resulting in less enforcement on Young's modulus compared to that of 7.0 wt% CNF. These were also the fracture initiating points that resulted in decreasing strengths in PLA films. Although the critical concentration for CNF agglomeration varies because of the variation of material properties, CNF agglomeration is always observed after the formation of the CNF network (Iwatake et al., 2008; Xu et al., 2013). From our data, Young's modulus of PU/CNF nanocomposite films reached its maximum when 2.0 wt% CNF was added to the PU matrix. According to the literature, the agglomeration must come after the formation of the CNF network. We hypothesized that the formation of the CNF agglomerate might happen between 2.0–4.0 wt%, and the mesh size of the CNF network shrunk to a level that constrained PU from phase separation at 4.0 wt% CNF. The heterogeneous distribution of CNF also led to the decreased Young's modulus on the PU/CNF-4.0 film. The CNF network, standing on the assumption of CNF agglomeration, probably formed before the CNF weight ratio reached 2.0 wt%. In the following

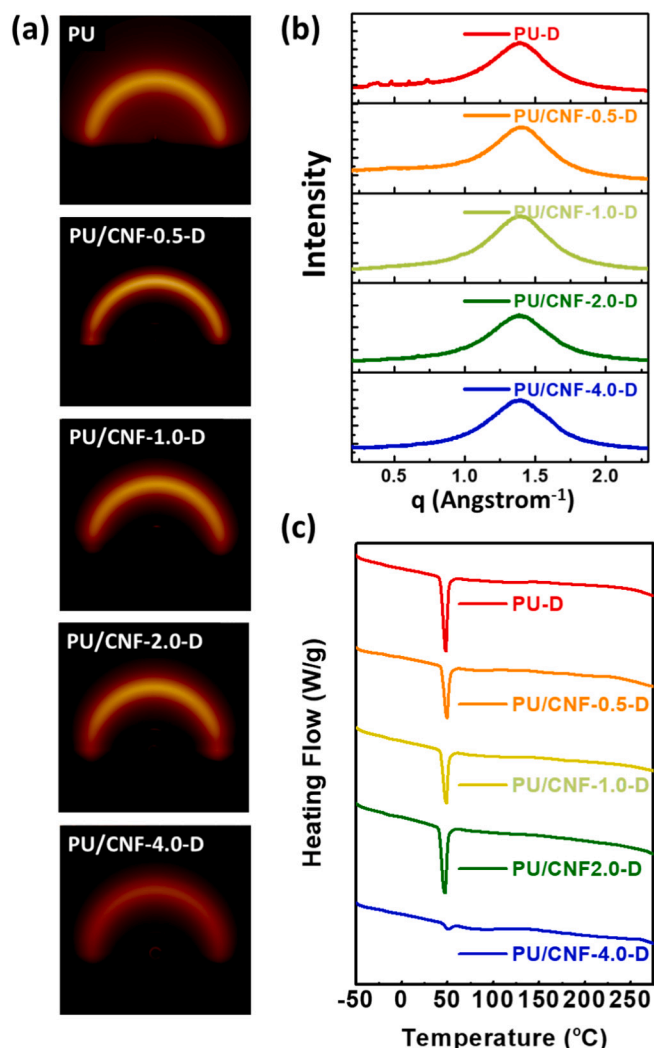


Fig. 3. Morphology studies of PU/CNF nanocomposite films. (a) 2D GIWAXS (b) integrated GIWAXS intensity versus  $q$  value. (c) DSC results at the first heating scan.

section, the characterization of electrospun PU/CNF scaffolds sheds light on this unresolved question. Overall, CNF heterogeneously blended in the PU matrix, promoting a significant increase in Young's modulus and tensile strength of the PU composite. Higher-order microstructure constructed by CNF led to a non-linear correlation between composition and mechanical strength. In summary, CNF is a very effective component for increasing the tensile strength of PU without scarifying the strain rate. The tensile strength of PU/CNF-2.0 was comparable to that of PU/EC-70. On the contrary, the elongation of PU/CNF-2.0 was almost two orders larger than that of PU/EC-70. The molecular arrangement in the composite plays a key role in determining the mechanical properties.

### 3.3. Microstructure and mechanical properties of electrospun PU/EC nanocomposite scaffolds

Electrospinning is a popular fabrication method for preparing scaffolds, a porous substrate, by applying an electric field between material-extruding syringe and collector to physically extract nano- to sub-micrometer filaments. Unlike the drop-casting films, the electrospun fibrous scaffolds of PU/EC can be fabricated into two distinct morphologies. Isotropic scaffolds comprise sub-micrometer fibers oriented almost randomly in all directions on the scaffold plane. On the other hand, anisotropic scaffolds are composed of fibers highly, but not

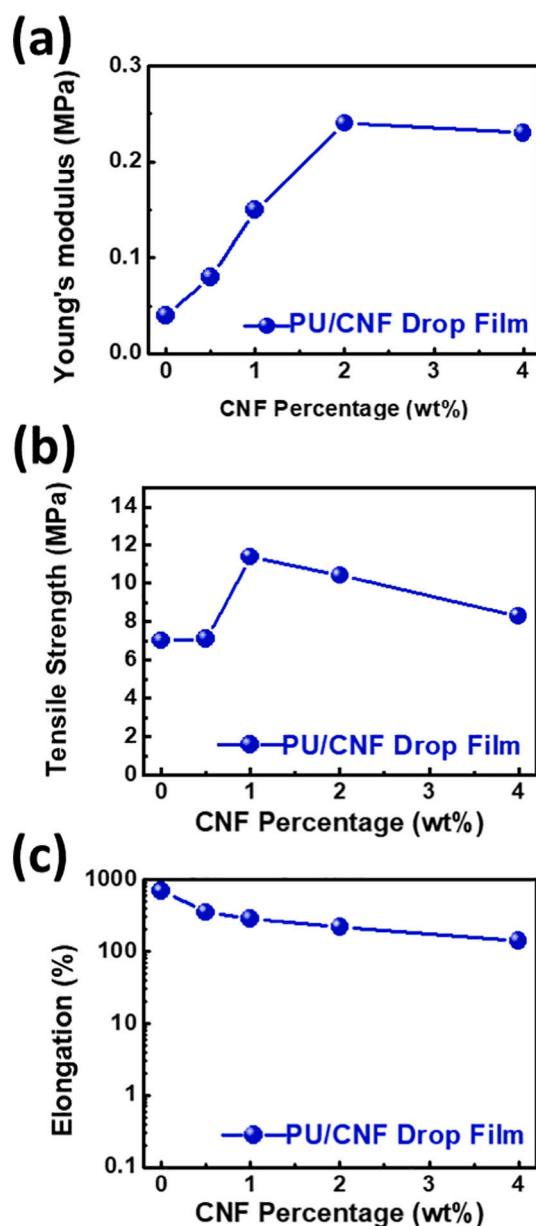


Fig. 4. Plots of mechanical properties versus various CNF concentrations of PU/CNF composite films (a) Young's modulus, (b) tensile strength, and (c) elongation.

entirely, aligned into one axis. Thus, the anisotropic scaffold is fabricated through two shear forces, one from the fiber formation and the other from fiber winding. Their crystalline structures are evaluated by WAXS. The degree of alignments is calculated and compared to the drop-casting film, shown in Fig. 5.

Fig. 5(a) shows the integrated intensity versus  $q$  value of each sample. Two crystallization signals of PU around 1.52 and 1.67 Å, embedded in the hallow background, are shown in the anisotropic electrospun scaffold of pure PU. The two peaks can be confirmed to be signals representing PU crystals (Camarena-Maese et al., 2020). The polymer undergoes heavy shearing force during the electrospinning process of the anisotropic scaffold, resulting in a high degree of PU crystalline, shown as sharp signals in WAXS. The absence of PU crystalline signals in the drop-casted film and the isotropic electrospun scaffold indicates that intense shearing is essential for the crystallization of PU. The crystalline PU was only presented in anisotropic PU/EC scaffolds containing less than 30.0 wt% EC. No significant crystalline signal was observed for PU/

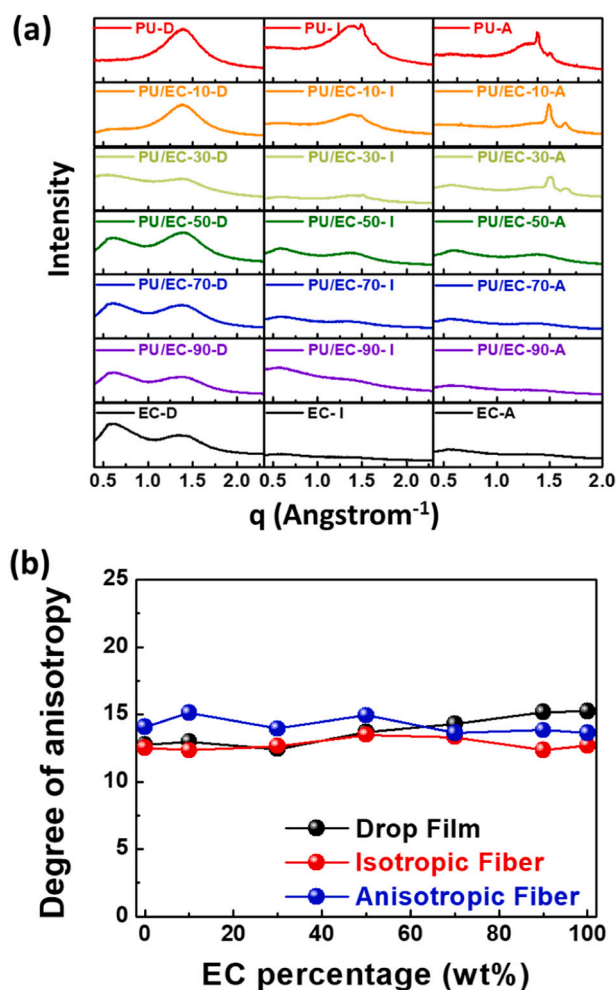


Fig. 5. (a) Integrated GIWAXS intensity versus  $q$  value of PU/EC composite scaffolds fabricated by three methods. (b) Degree of anisotropy of PU/EC composite scaffolds. The degree of anisotropy is defined as the ratio of integrated GIWAXS intensity in the y-axis ( $\pm 10^\circ$  azimuth angle) to total intensity.

EC scaffolds containing more than 50.0 wt% EC or pure EC scaffold. The results suggest that EC prefers not to form crystals and curbs the formation of PU crystals to some degree. The orientation of the signal around 1.4 Å in WAXS was calculated and plotted versus EC weight ratio, shown in Fig. 5(b). The properties of PU/EC films and scaffolds are summarized in Table S3. Although an external force is extensively applied to the PU/EC composite during electrospinning, the signal of WAXS does not concentrate in certain directions. It implies that the orientation of microstructures, including PU crystals and separated phases, is uniformly distributed in an azimuth angle with no preferred direction after an external force is applied. In summary, the macroscopic anisotropic PU/EC scaffolds do not exhibit molecular anisotropic preferred orientation even under severe shear force.

The tensile tests were used to evaluate the mechanical properties of three PU/EC composite scaffolds, and the results are shown in Fig. 6. The elastic properties of the PU/EC-50 samples prepared under different processing conditions were represented by their stress-strain curves as shown in Fig. S2. The Young's modulus, tensile strength, and elongation of PU/EC nanocomposite scaffolds are listed in Table S3. The values listed in the table were obtained from the average data of the measurement from three samples of each material.

Other than PU/EC-50, electrospinning has little effect on enhancing the elasticity and maximum PU/EC composite tensile strength. Both isotropic and anisotropic electrospun PU/EC-50 scaffolds show surprisingly high modulus and tensile strength. Both DSC and WAXS reveal

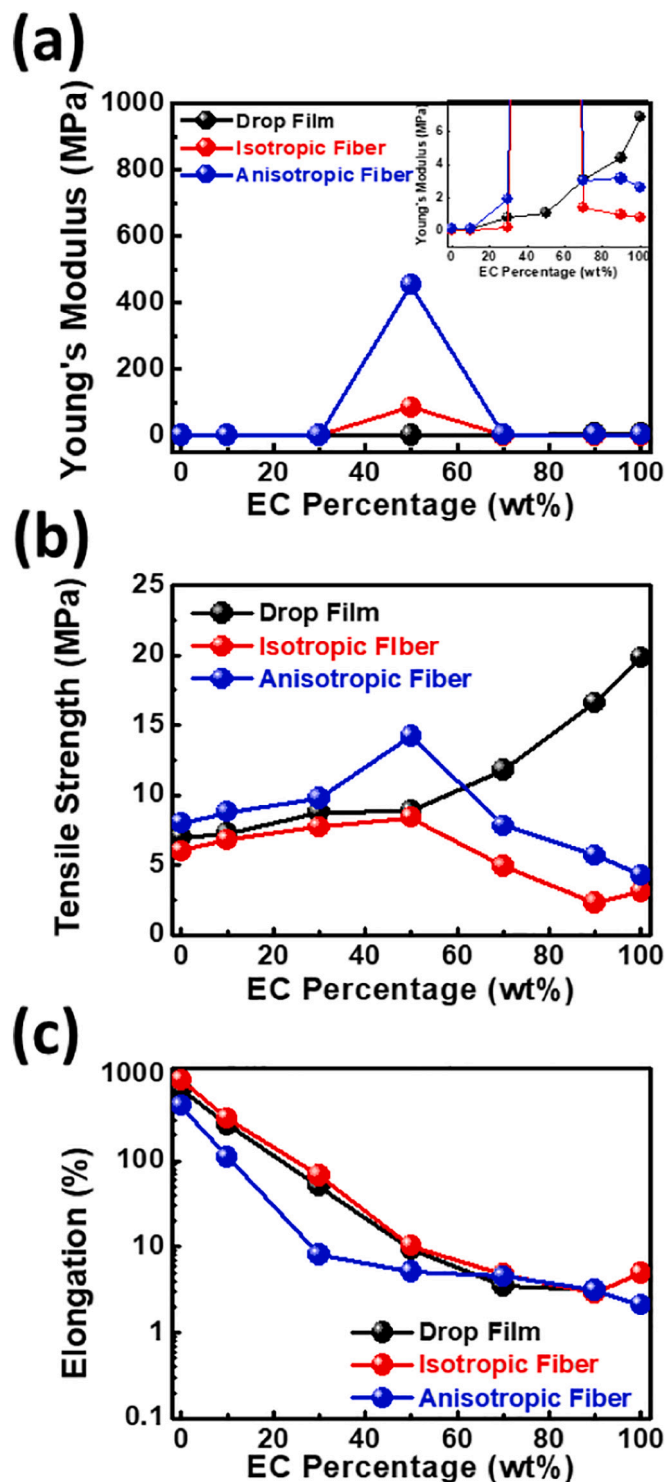


Fig. 6. Plots of mechanical properties versus EC weight ratio in PU/EC composite scaffolds. (a) Young's modulus (b) tensile strength, and (c) elongation.

no significant microstructural changes that can account for such abnormally high modulus. In thermogravimetric analysis, PU/EC-50 showed a relatively high degree of decomposition ( $T_d$ ) than all scaffolds with other compositions (Fig. S3). As mentioned in solid-state NMR (Fig. S1), an equal amount of PU and EC could have exceptional interaction and form a homogeneously mixed phase with exceptional stiffness. We speculate that the exceptional stiffness is due to the presence of crystalline PU and the intimate molecular interaction at the blending weight ratio at or below 1:1. This phenomenon warrants more future

studies.

Compared to drop-casted films, electrospun scaffolds are expected to exhibit high modulus due to increased polymer crystallinity by shearing force. However, only the anisotropic scaffold containing less than 70.0 wt% EC exhibited a higher modulus than their corresponding drop-casted films. The different orientations of sub-micrometer fibers in both anisotropic and isotropic scaffolds may produce mixed results in tensile testing. Unexpectedly, the modulus and tensile strength of both anisotropic and isotropic electrospun scaffolds containing higher than 70.0 wt% EC were notably lower than their corresponding drop-casted films. In one instance, the modulus and tensile strength of electrospun scaffolds were only one-third to one-fourth of their corresponding drop-casted film. The calculated porosities of electrospun scaffolds (Table S4) did not correlate with their mechanical strength, suggesting the porous structure did not account for decreased modulus and tensile strength. From SEM images, surface defects were not observed in all electrospun PU/EC scaffolds, but changes in fiber morphology were observed as the EC weight ratio increased (Fig. S5). For scaffolds containing less than 50.0 wt% EC, the fibers were curled and interconnected due to the elasticity of PU. On the contrary, in scaffolds with more than 50.0 wt% EC, no fibers were interconnected, and the fiber diameter was smaller than that with a low EC content. Therefore, the drop in tensile strength and modulus of scaffolds with more than 50.0 wt% EC might result from the morphological change in their microfibril mat.

### 3.4. Microstructure and mechanical properties of electrospun PU/CNF nanocomposite scaffolds

The crystallization of PU assisted by shearing force is a widely accepted fact, though how the cellulose nano-additives influence this shearing-assisted crystallization of PU remains unclear. Donglin Tian et al. reported the PU-grafted CNC exhibited better alignment toward the shearing direction (Tian et al., 2019). Still, the correlation between CNC and shear-assisted crystallization of PU was not addressed. Here, we investigated three types of drop-casted PU/CNF films and two types of electrospun PU-CNF nanocomposite scaffolds using various degrees of shearing. They were characterized by GIWAXS to reveal the role of CNF in PU phase separation and crystallization under the shearing process. The GIWAXS intensity versus  $q$  is shown in Fig. 7(a).

Despite CNF's inability to promote PU crystallization in the drop-casted film, the addition of CNF drastically enhanced the crystallinity of PU under the shearing process. This phenomenon has never been reported in PU/nanocellulose composites. These PU/CNF nanocomposite scaffolds present extremely strong scattering signals at 1.5 and 1.6 Å, which corresponds to the characteristic peaks of PU crystallization. This enhancement in PU crystallization reached its maximum efficacy when the nanocomposite comprises 1.0 wt% CNF. For PU/CNF scaffolds with higher than 1.0 wt% CNF, the signal of PU crystals and the hallow background of phase separation significantly decreased. The orientation of polymer chains, shown in Fig. 5(b), correlated with the CNF weight ratio. The PU chains had the highest degree of alignment in PU/CNF-1.0 compared to other compositions. The requirement of a large shearing force for PU crystallization and the microstructure study on PU/CNF film revealed how CNF interacts with PU under the shearing process.

As discussed before, the crystallization of PU only happened under an intense shearing process such as electrospinning. Although additive-assisted crystallization of PU has been addressed in the MWCNT and graphene nanocomposite system (Hosseini-Sianaki et al., 2015; Landa et al., 2014), the decreased modulus of PU/CNF-4.0 suggested a different PU/CNF nanocomposite formation mechanism in this research. We hypothesize that, during electrospinning, dispersed CNF exhibits good alignment to the shearing force. Then, with the guidance of CNF, PU polymer chains can align to the shearing direction and form compact packing of crystal. However, as the literature suggests, CNF will form its network and agglomeration when its weight ratio exceeds a critical

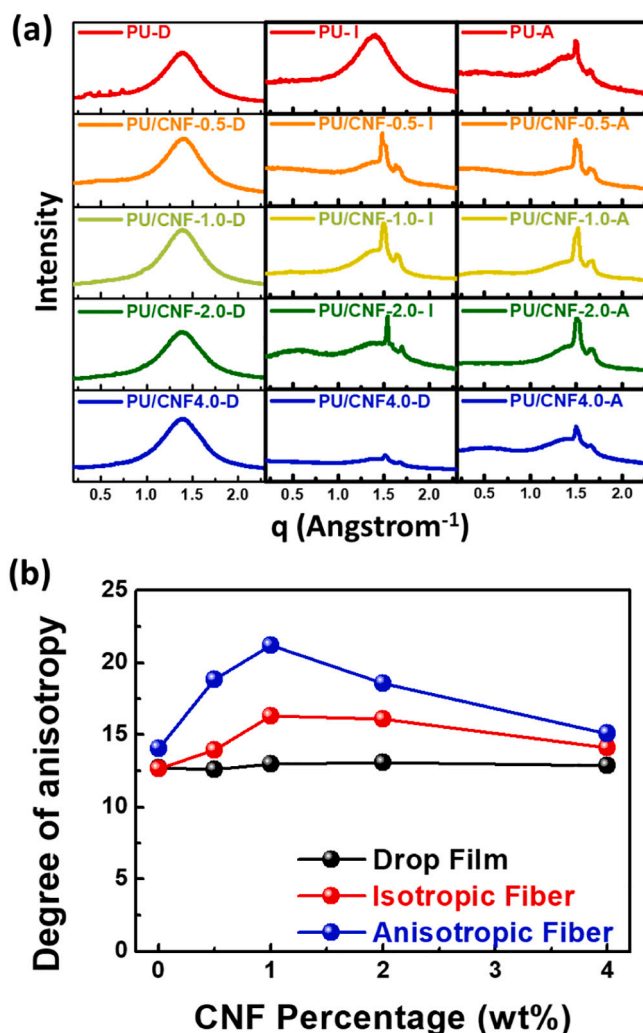


Fig. 7. (a) Integrated GIWAXS intensity versus  $q$  value of PU/CNF composite scaffolds fabricated using three methods. (b) Degree of anisotropy of PU/CNF composite scaffolds. The degree of anisotropy is defined as the ratio of integrated GIWAXS intensity in the  $y$ -axis ( $\pm 10^\circ$  azimuth angle) to total intensity.

value (Cheng et al., 2016; Iwatake et al., 2008; Xu et al., 2013). The critical concentration for the CNF network formation might be between 1.0 and 2.0 wt%. Because of the entanglement between fibers, CNF within its network and agglomeration can hardly be aligned with the shearing force, leading to a lower molecular alignment of PU and its crystallinity. Following the previous section's hypothesis about the PU/CNF drop-casted films, CNF forms agglomeration when the CNF exceeds 2.0 wt%. The two hypotheses are consistent, pointing to the formation of CNF agglomeration always comes after the formation of the CNF network (Seddiqi et al., 2021; Su et al., 2016; Zuo et al., 2018).

The mechanical properties of PU/CNF nanocomposite scaffolds are largely enhanced from the crystallization of PU induced by CNF under the shear force. The tensile testing results of PU/CNF nanocomposite scaffolds prepared by three fabrication processes are shown in Fig. 8. The elastic properties of the PU/CNF-1.0 samples prepared under different processing conditions were represented by their stress-strain curves as shown in Fig. S4. The Young's modulus, tensile strength, and elongation of PU/CNF-1.0 nanocomposite scaffolds are listed in Table S5. The listed values in the table were obtained from the average data of the measurements from three samples of each material.

The correlation between the CNF weight ratio and Young's modulus was similar to the observation of crystallinity and degree of anisotropy from WAXS. The consistency of the mechanical properties and WAXS

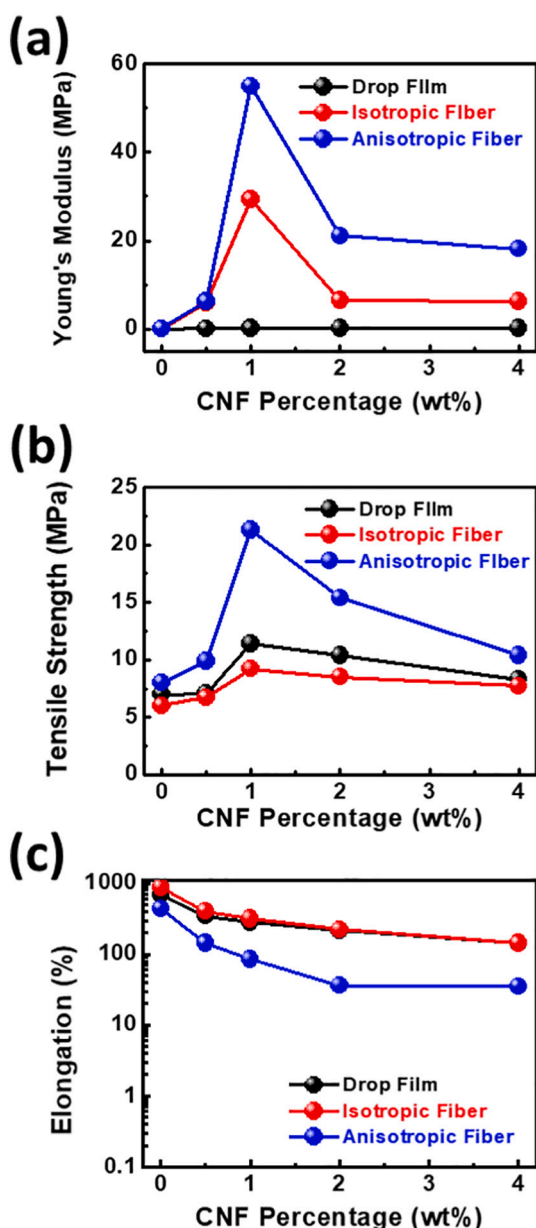


Fig. 8. Plots of mechanical properties versus CNF weight ratio in PU/CNF composite scaffolds. (a) Young's modulus, (b) tensile strength, and (c) elongation.

agreed with our two hypotheses on the intricate role of CNF in the PU/CNF network and agglomerated structure. Notably, Young's moduli of CNF-containing nanocomposites are significantly enhanced by one to two orders while maintaining their tensile strength and elongation. The PU/CNF-1.0 scaffolds had the largest degree of improvement in Young's modulus, from 0.15 to 54.95 MPa, which is the best of all samples. More importantly, while the PU/EC samples containing less than 10.0% EC had comparable modulus and tensile strength to the electrospun PU/CNF-1.0 sample, the PU/CNF-1.0 retained more than 70.0% of strain rate at the same time. The outstanding balanced properties of moduli, tensile strength, and elongation made these electrospun PU/CNF nanocomposite scaffolds prospective materials in many different applications, especially in regenerative bio-scaffolds for stiff tissues such as cardiac muscles and cartilages (Chen et al., 2015; Chen et al., 2019; Xu et al., 2020).

Fig. 9 visualizes the relation between the elongation and tensile strength of PU scaffolds with cellulose-derived additives via different

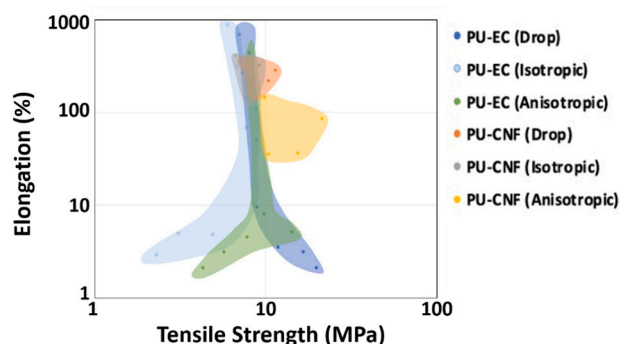


Fig. 9. A plot of elongation and tensile strength of PU/EC and PU/CNF composites fabricated using three methods.

processes mentioned in this work. The PU/EC composite scaffolds have a clear elongation and tensile strength trade-off trend. The elongation of PU/EC film composite has plummeted when the tensile strength is enhanced by blending EC. For electrospun PU/EC scaffolds, a region reaching the left-bottom part of the diagram indicates dropped tensile strength and elongation of scaffolds. These intriguing results are likely caused by the morphological change of various electrospun scaffold compositions.

On the other hand, the data points for PU/CNF composites with relatively low CNF weight ratios are located in a more focused area in this plot. Another reason is that the network and agglomeration of CNF inhibit the mechanical reinforcement of CNF after its weight ratio exceeds a critical concentration. The shearing process significantly affects PU/CNF nanocomposites compared to PU/EC composites. While drop-casted PU/EC films share almost the same area as their corresponding isotropic and anisotropic scaffolds, the region of anisotropic PU/CNF scaffolds (deep yellow) does not overlap with the area of drop-casted PU/CNF films (orange). It highlights the unique microstructural change of PU/CNF nanocomposite under extensive shearing, leading to much improved tensile strength while maintaining a reasonable strain rate. This plot shows the fundamental difference in mechanical tuning resulting from cellulose-additive's morphological characteristics and their roles during materials fabrication.

### 3.5. A model for the microstructure formation of PU/cellulose composites

Finally, we propose a model to reveal the roles of different types of cellulose and their composition in tuning the microstructure of the PU matrix with and without shearing force, as shown in Fig. 10. While EC mixes well with PU on the molecular scale and reduces the phase separation of PU, less than 2.0 wt% CNF has little interference with the microstructure of PU. The formation of the CNF network begins when the CNF weight ratio reaches between 1.0 and 2.0 wt%, but it leaves sufficient space for PU chain movement to form the separated phase. When the CNF weight ratio reaches 4.0 wt%, it forms a dense network and partially flocculates, confining the movement of the PU polymer chains. For the cases under the shearing force, a low degree of PU crystalline is found in PU/EC composite scaffolds with less than 50.0 wt % EC.

On the other hand, the well-dispersed CNF supports PU crystallization by guiding the orientation of the polymer chains to align with the shearing direction. However, for greater than 1.0 wt% CNF, it forms networks that cannot align well with shearing force, providing less support for polymer chain alignment and PU crystallization. The confinement of the CNF network also makes phase separation of PU unfavorable. For PU/CNF-4.0, both the separated and crystal phase of PU are largely suppressed and disappear in DSC and WAXS. The characteristics of cellulose, its weight ratio, and the fabrication method all contribute to the morphologies and mechanical properties of the final

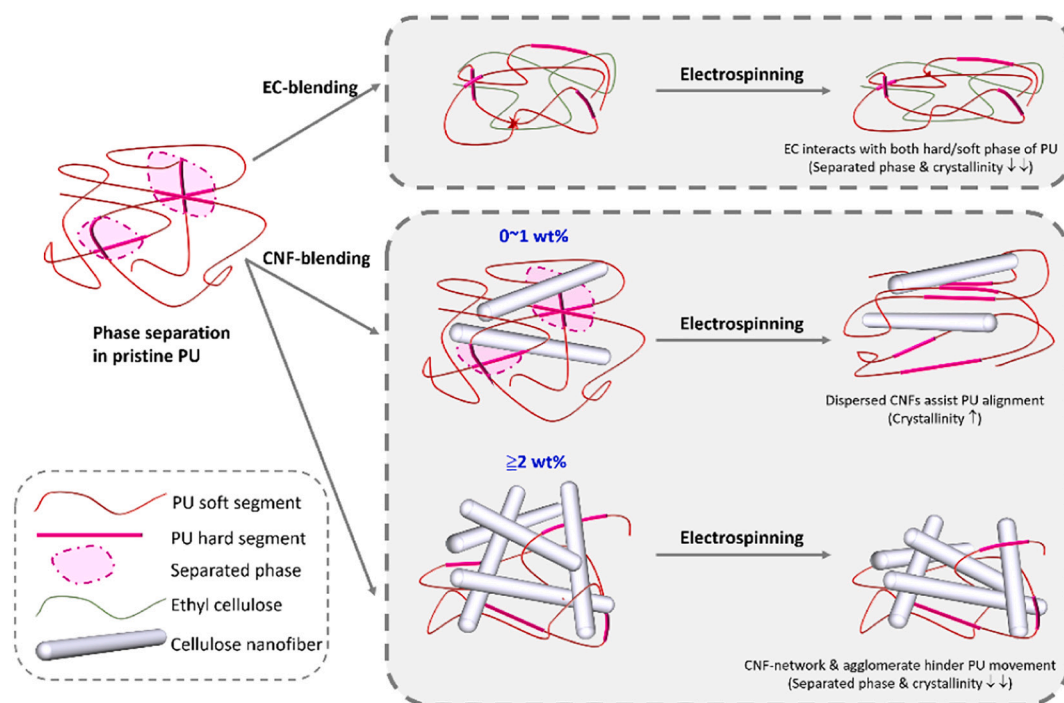


Fig. 10. A schematic diagram of the microstructure formation mechanism of PU/cellulose composites.

composites.

#### 4. Conclusion

In this study, the effect of various cellulose types, their weight ratios, and fabrication methods on PU microstructure was investigated and correlated to the mechanical properties of PU/cellulose composites. For PU/EC polymer blended films, the two polymers are mutually miscible, and EC suppresses the phase separation of PU. The addition of EC significantly improved Young's modulus and reduced the strain rate simultaneously. The addition of less than 2.0 wt% CNF had an undetectable effect on the microstructure of PU/CNF composite films before forming a dense CNF network, which somewhat confined the PU polymer chain. The non-linear effect on PU microstructure in PU/CNF composites emphasized the morphological differences between a polymeric derivative (EC) and a nanomaterial additive (CNF). Under a shearing process, well-dispersed CNF helped the PU chains align to the shearing direction, drastically enhancing the degree of PU crystalline and improving Young's modulus of electrospun PU/CNF scaffolds by more than two orders. With an excellent Young's modulus, electrospun PU/CNF scaffolds maintained a reasonable strain rate as well. A new mechanism of CNF promoting PU crystallization under a shearing process has been reported for the first time. The differences in PU microstructures with respect to the types of cellulose additives, their weight ratios, and fabrication methods have been summarized in this proposed model, providing a comprehensive understanding of the composition-structure relationship of PU composite materials. The findings provide a guideline for designing composite materials containing cellulose additives for desired mechanical properties that fit their roles in targeted applications.

#### CRediT authorship contribution statement

**Tzu-Yi Yu:** Investigation, Writing – original draft. **Yu-Kai Tseng:** Investigation. **Ting-Han Lin:** Investigation, Resources. **Tzu-Chia Wang:** Investigation. **Yun-Hsiu Tseng:** Investigation. **Yin-Hsuan Chang:** Investigation, Writing – review & editing. **Ming-Chung Wu:**

Methodology, Writing – review & editing. **Wei-Fang Su:** Conceptualization, Methodology, Writing – review & editing, Funding acquisition, Supervision.

#### Declaration of competing interest

The authors declare that they have no known competing financial interests or personal relationships that could have appeared to influence the work reported in this paper.

#### Acknowledgement

This research is granted by the Ministry of Science and Technology, Taiwan, under the project number: MOST 108-2221-E-002-027-MY3 and 110-2628-E-182-001. The authors also thank the Chang Gung University (QZRPD181) and Chang Gung Memorial Hospital at Linkou (CMRPD2L0081 and BMRPC74) for financial support. We appreciate Prof. Kimura from Kyoto University for supporting the solid-state NMR analysis of PU/ED polymer blend, and the National Synchrotron Radiation Research Center (NSRRC) for supporting Small Angle X-ray Scattering (SAXS) and Wide Angle X-ray Scattering (WAXS) facilities.

#### Appendix A. Supplementary data

Supplementary data to this article can be found online at <https://doi.org/10.1016/j.carbpol.2022.119549>.

#### References

- Basu, A., Lindh, J., Ålander, E., Strømme, M., & Ferraz, N. (2017). On the use of ion-crosslinked nanocellulose hydrogels for wound healing solutions: Physicochemical properties and application-oriented biocompatibility studies. *Carbohydrate Polymers*, 174, 299–308.
- Camarena-Maese, F. J., Martínez-Hergueta, F., Fernández-Blázquez, J. P., Kok, R. W., Reid, J., & Callanan, A. (2020). Multiscale SAXS/WAXD characterisation of the deformation mechanisms of electrospun PCL scaffolds. *Polymer*, 203, Article 122775.
- Chen, P.-H., Liao, H.-C., Hsu, S.-H., Chen, R.-S., Wu, M.-C., Yang, Y.-F., & Su, W.-F. (2015). A novel polyurethane/cellulose fibrous scaffold for cardiac tissue engineering. *RSC Advances*, 5(9), 6932–6939.

- Chen, R.-D., Huang, C.-F., & Hsu, S.-H. (2019). Composites of waterborne polyurethane and cellulose nanofibers for 3D printing and bioapplications. *Carbohydrate Polymers*, 212, 75–88.
- Cheng, D., Wen, Y., An, X., Zhu, X., & Ni, Y. (2016). TEMPO-oxidized cellulose nanofibers (TOCNs) as a green reinforcement for waterborne polyurethane coating (WPU) on wood. *Carbohydrate Polymers*, 151, 326–334.
- Chu, Y., Sun, Y., Wu, W., & Xiao, H. (2020). Dispersion properties of nanocellulose: A review. *Carbohydrate Polymers*, 250, Article 116892.
- Fox, S. C., Li, B., Xu, D., & Edgar, K. J. (2011). Regioselective esterification and etherification of cellulose: A review. *Biomacromolecules*, 12(6), 1956–1972.
- Hosseini-Sianaki, T., Nazockdast, H., Salehnia, B., & Nazockdast, E. (2015). Microphase separation and hard domain assembly in thermoplastic polyurethane/multiwalled carbon nanotube nanocomposites. *Polymer Engineering and Science*, 55, 2163–.
- Iwatake, A., Nogi, M., & Yano, H. (2008). Cellulose nanofiber-reinforced polylactic acid. *Composites Science and Technology*, 68(9), 2103–2106.
- Landa, M., Canales, J., Fernández, M., Muñoz, M. E., & Santamaría, A. (2014). Effect of MWCNTs and graphene on the crystallization of polyurethane based nanocomposites, analyzed via calorimetry, rheology and AFM microscopy. *Polymer Testing*, 35, 101–108.
- Liang, J.-Z., & Ma, W.-Y. (2012). Young's modulus and prediction of plastics/elastomer blends. *Journal of Polymer Engineering*, 32(6–7), 343–348.
- Lin, T. H., Liao, Y. H., Lee, K.-M., Chang, Y. H., Hsu, K.-H., Hsu, J.-F., & Wu, M.-C. (2021). Organic solvent resistant nanocomposite films made from self-precipitated Ag/TiO<sub>2</sub> nanofibers and xellulose nanofiber for harmful volatile organic compounds photodegradation. *Advanced Materials Interfaces*, 8, 2101467.
- Lu, Y., & Yuan, W. (2018). Superhydrophobic three-dimensional porous ethyl cellulose absorbent with micro/nano-scale hierarchical structures for highly efficient removal of oily contaminants from water. *Carbohydrate Polymers*, 191, 86–94.
- Mao, D., Li, Q., Bai, N., Dong, H., & Li, D. (2018). Porous stable poly(lactic acid)/ethyl cellulose/hydroxyapatite composite scaffolds prepared by a combined method for bone regeneration. *Carbohydrate Polymers*, 180, 104–111.
- Nishiyama, Y., Langan, P., & Chanzy, H. (2002). Crystal structure and hydrogen-bonding system in cellulose I $\beta$  from synchrotron X-ray and neutron fiber diffraction. *Journal of the American Chemical Society*, 124(31), 9074–9082.
- Nishiyama, Y., Sugiyama, J., Chanzy, H., & Langan, P. (2003). Crystal structure and hydrogen bonding system in cellulose I $\alpha$  from synchrotron X-ray and neutron fiber diffraction. *Journal of the American Chemical Society*, 125(47), 14300–14306.
- Pei, A., Malho, J.-M., Ruokolainen, J., Zhou, Q., & Berglund, L. A. (2011). Strong nanocomposite reinforcement effects in polyurethane elastomer with low volume fraction of cellulose nanocrystals. *Macromolecules*, 44(11), 4422–4427.
- Redondo, A., Mortensen, N., Djeghdi, K., Jang, D., Ortuso, R. D., Weder, C., & Gunkel, I. (2022). Comparing percolation and alignment of cellulose nanocrystals for the reinforcement of polyurethane nanocomposites. *ACS Applied Materials & Interfaces*, 14(5), 7270–7282.
- Saito, T., Kimura, S., Nishiyama, Y., & Isogai, A. (2007). Cellulose nanofibers prepared by TEMPO-mediated oxidation of native cellulose. *Biomacromolecules*, 8(8), 2485–2491.
- Sakakibara, K., Yano, H., & Tsujii, Y. (2016). Surface engineering of cellulose nanofiber by adsorption of diblock copolymer dispersant for green nanocomposite materials. *ACS Applied Materials & Interfaces*, 8(37), 24893–24900.
- Seddiqi, H., Oliaei, E., Honarkar, H., Jin, J., Geonzon, L. C., Bacabac, R. G., & Klein-Nulend, J. (2021). Cellulose and its derivatives: Towards biomedical applications. *Cellulose*, 28(4), 1893–1931.
- Su, W.-F., Ho, C.-C., Shih, T.-H., Wang, C.-H., & Yeh, C.-H. (2016). Exceptional biocompatibility of 3D fibrous scaffold for cardiac tissue engineering fabricated from biodegradable polyurethane blended with cellulose. *International Journal of Polymeric Materials and Polymeric Biomaterials*, 65(14), 703–711.
- Tian, D., Wang, F., Yang, Z., Niu, X., Wu, Q., & Sun, P. (2019). High-performance polyurethane nanocomposites based on UPy-modified cellulose nanocrystals. *Carbohydrate Polymers*, 219, 191–200.
- Xu, C.-A., Nan, B., Lu, M., Qu, Z., Tan, Z., Wu, K., & Shi, J. (2020). Effects of polysiloxanes with different molecular weights on in vitro cytotoxicity and properties of polyurethane/cotton–cellulose nanofiber nanocomposite films. *Polymer Chemistry*, 11(32), 5225–5237.
- Xu, X., Liu, F., Jiang, L., Zhu, J. Y., Haagenson, D., & Wiesenborn, D. P. (2013). Cellulose nanocrystals vs. cellulose nanofibrils: A comparative study on their microstructures and effects as polymer reinforcing agents. *ACS Applied Materials & Interfaces*, 5(8), 2999–3009.
- Ye, D., Yang, P., Lei, X., Zhang, D., Li, L., Chang, C., & Zhang, L. (2018). Robust anisotropic cellulose hydrogels fabricated via strong self-aggregation forces for cardiomyocytes unidirectional growth. *Chemistry of Materials*, 30(15), 5175–5183.
- Yuan, B., Sun, H., Wang, T., Xu, Y., Li, P., Kong, Y., & Niu, Q. J. (2016). Propylene/propane permeation properties of ethyl cellulose (EC) mixed matrix membranes fabricated by incorporation of nanoporous graphene nanosheets. *Scientific Reports*, 6(1), 28509.
- Zuo, X., Wu, J., Ma, X., Deng, X., Cai, J., Chen, Q., & Nan, J. (2018). A poly(vinylidene fluoride)/ethyl cellulose and amino-functionalized nano-SiO<sub>2</sub> composite coated separator for 5 V high-voltage lithium-ion batteries with enhanced performance. *Journal of Power Sources*, 407, 44–52.